Available online at www.sciencedirect.com

ScienceDirect

journal homepage: www.elsevier.com/locate/he



High-fidelity H_2–CH_4 jet in crossflow modelling with a flame index-controlled artificially thickened flame model

Simone Castellani [a,*], *Roberto Meloni* [b], *Stefano Orsino* [c], *Naseem Ansari* [c], *Rakesh Yadav* [c], *Didier Bessette* [c], *Isaac Boxx* [d,e], *Antonio Andreini* [a]

[a] *Department of Industrial Engineering DIEF, University of Florence, Via di Santa Marta 3, Florence 50139, Italy*
[b] *Nuovo Pignone Tecnologie s.r.l, Baker Hughes, Via Felice Matteucci 2, Florence 50127, Italy*
[c] *Ansys, Inc., USA*
[d] *Institute of Combustion Technology, German Aerospace Center Stuttgart, Germany*
[e] *Chair of Optical Diagnostics in Energy, Chemical and Process Engineering RWTH Aachen University Aachen, Germany*

HIGHLIGHTS

- A novel skeletal chemical kinetic scheme for the H2–CH4 combustion has been derived.
- A H2–CH4 jet flame in crossflow has been numerically investigated.
- Validation of the artificially thickened flame model with the flame index correction.
- The change in the flame anchoring induced by the H2 addition has been captured.
- The role of the thickening on the multi regime flame front has been investigated.

ARTICLE INFO

Article history:
Received 15 December 2022
Received in revised form
17 April 2023
Accepted 19 May 2023
Available online 15 June 2023

Keywords:
Multi-regime combustion modelling
Artificially thickened flame model
Jet in crossflow flame
Hydrogen-methane combustion modelling

ABSTRACT

Hydrogen introduction in existing combustion systems can heavily alter the flame morphology and stability limit of the system itself. This makes the numerical prediction of such changes crucial for the development of effective design modifications. In the industrial framework, often it is required to have combustion models capable of handling both the premixed and the diffusive combustion regimes and this represents a real modelling challenge. In this work, a multi-regime CH4–H2 Jet In Crossflow (JICF) flame, at gas turbine relevant conditions, has been investigated with a Flame Index controlled Artificially Thickened Flame Model (ATFM). The numerical prediction shows good agreement with the detailed experimental data from DLR laboratory, and the model has been found to correctly predict the change in the flame anchoring topology due to an increase of H2 content.
© 2023 The Authors. Published by Elsevier Ltd on behalf of Hydrogen Energy Publications LLC. This is an open access article under the CC BY license (http://creativecommons.org/licenses/by/4.0/).

* *Corresponding author.*
E-mail address: simone.castellani@unifi.it (S. Castellani).
https://doi.org/10.1016/j.ijhydene.2023.05.210
0360-3199/© 2023 The Authors. Published by Elsevier Ltd on behalf of Hydrogen Energy Publications LLC. This is an open access article under the CC BY license (http://creativecommons.org/licenses/by/4.0/).

Introduction

The Jet In Cross Flow (JICF) is one of the most extensively studied flow field configurations in fluid dynamics, it is indeed one of the most common flow structures used to promote mixing between separate streams. In Gas Turbine (GT) combustion applications, JICF is used either to realize stable anchoring of the flame around fuel jets [1] or to promote the premixing of the fuel-air mixture. In any case, this flow structure is historically well known for its mixing-enabling capacity. Considering the very similar jet in co-flow configuration, the mechanism that induces the turbulent mixing is reduced to the Kelvin Helmholtz instabilities which are generated along the shear layer [2]. In addition to these, the JICF flow field is characterized by other coherent vortex structures: the counter-rotating vortex pair, the horseshoe vortices, and wake vortices [3–6], which are in turn additional mixing sources. The penetration of JICF has been characterized through the definition of the momentum ratio non-dimensional parameter ($r = \sqrt{\rho_j u_j^2 / \rho_c u_c^2}$) [6], which allows the formulation of a very simple power-low correlation describing the jet centerline trajectory [6].

To offset the hazardous effects of climate change, there is an urgent need to assess the fuel worthiness of alternate fuels. Hydrogen as an alternate fuel, provides a promisng future but the transition from fossil fuel to hydrogen has to be carefully considered. In the first phase of the energy transition scenario, H2 will be progressivly added to the existing fossil fuel and it is therefore expected that the power generation sector will see the necessity of using H2/CH4 blends. In this framework, the study of the anchoring characteristics of an H2/CH4 JICF can have a direct impact on several design aspects related to GT combustors, ranging from the mitigation of the pollutant emissions (i.e., NO_x and CO [7–9]) to the reduction of the damage risk that the hardware can face when the flame stabilizes around undesired locations in case of flashback events. In literature, H2 and H2/CH4 jet flow in a crossflow flame (JFICF) has been widely investigated experimentally [10–14]: Steinberg et al. [12] have studied an H2 JFICF at atmospheric pressure. Recently, Saini et al. [13,14] presented a series of extensive experimental work focused on an H2 and H2/CH4 confined JFICF at relatively high pressure and temperature. Regarding numerical studies on the H2-JFICF, Grout et al. [15,16] have presented some Direct Numerical Simulation (DNS) investigations in which they have analyzed the flame anchoring phenomenon and the effect of a change in the fuel injection angle on the flame-holding capability. However, moving towards a more cost-effective modelling strategy, the investigation of a JFICF flame configuration from the Computational Fluid Dynamic (CFD) perspective poses a real challenge. The combustion of fuel jets is an intrinsic transient phenomena in which the flame stabilization is controlled bymixing, the prediction of which is essential for an adequate description of the physics. Concerning the mixing prediction, Galeazzo et al. [17] showed the limitations of the existing RANS models in predicting the turbulent mixing characteristics of JICF. In this study, it is demonstrated that an LES approach is capable of satisfactorily predicting the flow field and the turbulent mixing associated with the velocity fluctuations. When dealing with reactive conditions, with hydrogen or blends of hydrogen with natural gas, the numerical limitations are more profound: Grout et al. [16] found that JICF hydrogen flames exhibit both diffusive and premixed combustion regimes and their relative occurrence is strictly linked with the type of anchoring mechanism. This aspect raises several modelling issues that are even amplified if H_2 is considered in a very high percentage. Indeed, the enhanced H_2 diffusivity requires a particular treatment of the preferential diffusion effects strongly limiting most of the simplifying, cost-effective, modelling assumptions on which several models are founded. To substantiate this assertion, H2-JFICF DNS investigations of Chan et al. [18] showed that the strong differential diffusion effects would play a key role in the flame anchoring mechanism. They demonstrated that the use of any flamelet combustion model for the description of such phenomena would require preferential diffusion effects to be accounted for.

By taking a step back and trying to summarize the possible modelling strategies available in literature, the existing turbulent combustion models can be divided into two main macro-categories: the first is based on the transport of the primitive variables (species transport models), and the second is on the transport of auxiliary scalars. The latter are often easily coupled with the flamelet assumption and the tabulated chemistry approach. The Flamelet Generated Manifold (FGM) model [19] is one of the most used approaches belonging to the second category. The feasibility of including preferential diffusion effects in the FGM model has been widely investigated in literature [20–25], and different authors have proposed different control variables and tabulation approaches incorporating the preferential diffusion for perfectly premixed cases. An additional modification has been proposed by Verhoeven et al. [26] in order to account for the preferential diffusion of H2 in the non-premixed environment. However, as pointed out by Pitsch et al. [27], the FGM model remains very dependent on the tabulated strategy that can involve premixed or diffusive laminar flamelet assumption. Different FGM formulations capable of characterizing multi-regime combustion have been presented by several authors [27–29] showing the advantages and the limitations of such hybrid approaches. However, the complexity of tabulated chemistry models grows significantly trying to include additional physics at the same time.

Regarding the "primitive variables" based approach, the preferential diffusion effects are intrinsically accounted for being the diffusivity of each species in the corresponding transport equation. The description of the turbulence chemistry interaction, in the species transport model, can be incorporated using different methods. In the framework of LES, one of the most used models is the Artificially Thickened Flame Model (ATFM) [30]. The ATFM is based on the concept of applying a uniform thickening factor to the premixed flame front that enables the flame resolution on the LES grid.In this model, an efficiency function plays the role of compensating the effect of the thickening in altering the Damkholer number. The original model has been adapted for the study of stratified flames and technically premixed flames by means of a dynamic thickening factor [31]. Compared to the original constant thickening model, the dynamic thickening applies the thickening only to the flame front chararterized by a flame sensor. This dynamic thickening approach allows the model

to not alter the diffusivity outside the flame front preserving a correct mixing field description. Nevertheless, the extension of this approach to non-premixed flames has been found theoretically unfeasible by De Luca [32]. In his work, it emerges clearly that there is no possibility of an extension of the classical thickening concept to diffusive flames. Indeed, any altering of the diffusivity results in a change of the global flame front fuel consumption that cannot be recovered through reaction source term scaling (in contrast to the premixed flames). Starting from the same statements, Cuenot et al. [33] investigated the possibility of applying a correction to the species diffusivity in order to compensate for the numerical diffusion induced by the mesh coarsening. However, this approach has been developed for laminar flames and cannot be directly extended to complex 3D turbulent flames. On the other hand, in literature, a widely adopted way to handle the diffusive part of the flame is to disable the thickening wherever the diffusive regime is observed. This assumption has proven to be effective for the description of several types of flames including spray based partially premixed gaseous flames [34,35]. This approach entrusts the resolution of the diffusive flame front solely to the computational grid resolution. A similar methodology has been used in the present work. In this context, the work aims to investigate the predictive capability of this modelling approach on a JICF flame. To accomplish this objective the JICF DLR test case has been numerically investigated to provide a model validation with respect to detailed experimental data [13] under gas turbine relevant conditions. The operating pressure, the fuel blends, and the temperature of the oxidizer considered in this experimental campaign are all relevant to gas turbine applications. In particular, a small addition of hydrogen, that moves the fuel mixture composition from low to medium H2 content, is sufficient to heavily impact the flame characteristics. In this sense, the work aims to reproduce the change in the flame anchoring topology experimentally observed and induced by the increase of the H2 content in the fuel mixture.

While in the next paragraph, the details of the turbulent combustion modelling approach will be presented, in Investigated Experimental Conditions the turbulent, reacting JICF test case is introduced with the details of the test points chosen for the model validation. The numerical setup and a brief description of the chemistry modelling approach are reported next. The results discussion is organized by presenting firstly a flow field prediction assessment, and secondly, the prediction comparison among the different modelling approaches and the experiments for the first test point. In the end, the lower H2 content test point is addressed focusing the discussion on the aspects that would have induced the change in the anchoring topology.

Turbulent combustion modelling

Partial premixing is observed in both non-premixed combustion when fuel and air mix without burning and in premixed combustion when the degree of reactant premixing is not perfect. One of the characterizing features of a premixed flame front is a limit on the reaction rate it exhibits in the form of a fixed propagating flame speed. On the other hand, non-premixed flames can theoretically exhibit infinitely fast chemistry (as in the Burke-Schumann limiting case [36]) but more often they burn with a finite rate on a non-propagating stoichiometric surface.

Turbulence has a major effect on the reaction rate, although it acts differently on premixed and non-premixed systems. In non-premixed cases, turbulence acts as a vehicle to bring fuel and oxidizers together for burning, and in premixed systems, turbulence can directly affect the flame structure and its propagation in case of modest and higher Karlovitz numbers [37]. Modelling non-premixed turbulent systems has been a challenge due to a lack of robust universal models for both premixed and non-premixed flames. Hydrogen flames are further complicated due to preferential diffusion effects [38]. The Artificially Thickened Flame Model [30] addresses the issue of a finite reaction rate/flame speed on an LES mesh by artificially thickening the unresolved thin flame front of the premixed system. The ATFM, in its dynamic formulation [31,39], introduces a dynamic thickening factor F, a flame sensor Ω, and an efficiency factor E in the species and energy equations.

$$\frac{\partial \overline{\rho}\,\tilde{\varphi}_\alpha}{\partial t}+\frac{\partial \overline{\rho}\,\tilde{u}_j\,\tilde{\varphi}_\alpha}{\partial x_j}=\frac{\partial}{\partial x_j}\left(\overline{\rho}(EFD_\alpha+(1-\Omega)D_t)\frac{\partial \tilde{\varphi}_\alpha}{\partial x_j}\right)+\frac{E}{F}\dot{\omega}_\alpha(\tilde{\varphi}) \tag{1}$$

In Eq. (1) the overbar represents the filtered quantity and tilde is the Favre filtered quantity. φ is the vector of N-species mass fractions and enthalpy. According to the formulation introduced by Legier et al. [31], the dynamic thickening factor F is evaluated as:

$$F=\Omega(F_{max}-1)+1 \tag{2}$$

where F_{max} is the local maximum thickening factor that is computed according to the local mixture composition and grid sizing (Δx) [39]:

$$F_{max}=\frac{\Delta x\, N_{Thick}}{D_{th}} \tag{3}$$

where D_{th} is thermal laminar flame thickness, which is preliminary tabulated as a function of the local mixture composition, and N_{Thick} is the number of grid points in the laminar flame thickness. The details of flame sensor Ω evaluation are given elsewhere [39] and not repeated here. The efficiency function requires estimation of the dilatation-free velocity fluctuation at the test filter. Colin et al. [30] have proposed a formulation that requires the third-order derivative of the filtered velocity, a non-trivial task on an unstructured mesh. Instead, the approach proposed by Durand et al. [40] is adopted here. Using a scale similarity assumption, the test filter velocity fluctuation is evaluated directly as

$$u'_{\Delta_e}=c\Delta|\nabla\times\tilde{u}-\nabla\times\widehat{\tilde{u}}| \tag{4}$$

where $\widehat{\tilde{u}}$ is the test-filtered velocity evaluated by averaging the velocity in the cells surrounding a given cell. As discussed earlier, the ATFM is strictly valid for premixed flames and does not apply to diffusion flames. Indeed, the thickening concept in premixed flames is based on the flame front fuel consumption proportionality with the diffusivity D_α and the rate $\dot{\omega}_\alpha(\tilde{\varphi})$ ($S_c\propto\sqrt{D_\alpha\dot{\omega}_\alpha(\tilde{\varphi})}$). This aspect makes it possible to alter the

diffusivity (FD_α) without altering the global fuel consumption across the flame front by applying a rate scaling $\dot{\omega}_\alpha(\tilde{\varphi})/F$. On the contrary, the fuel consumption of a diffusive flame front does not depend on the rate [33]; because of that, any scaling of the species diffusivity due to the thickening will result, in this case, in an alteration of the S_c. In order to avoid any local misprediction of the flame front fuel consumption, the premixed front has to be identified and modelled differently from the diffusive one. In this work, the Takeno flame index (*TI*) concept [28] is used to accomplish this task, and the formulation used for the fuel mixture considered is presented in Eq. (5). The normalized flame index (FI) takes a value of +1.0 in the premixed part of the flame and −1.0 in the non-premixed part.

$$TI = \nabla(Y_{CH4} + Y_{H2}) \bullet \nabla Y_{O2} \tag{5}$$

In the proposed model for partially premixed flames, the ATFM model is transitioned from the premixed front to a non-ATFM on the diffusion front using a delta function on *F*, Ω, and *E* directly. The model is addressed as FI-ATFM and is valid for a generic partially premixed system. This closure bases its validity on the intrinsic assumption that the diffusive front does not need any thickening to be solved. The latter assumption is not generally true; however, diffusive flames have higher stability resistance from the numerical perspective [33] with respect to the premixed ones. The latter aspect offers the possibility to solve these kinds of flames on LES grids without additional modelling assumptions. However, the extinction strain rate of the flame is heavily affected by the flame front discretization. In detail, a coarse grid is expected to induce higher numerical diffusion that contributes to reducing the extinction resistance of the diffusive flame front. Hence, the numerical prediction of the flame anchoring in the high strain rate regions is extremely challenging and requires an appropriate spatial discretization. Extinction is surely the higher impact effect that the no-modelling approximation brings with it but is not the only one. The presence of a certain amount of numerical diffusion due to the sub-optimal discretization of the flame front would lead to an uncontrolled overestimation of the local reactivity. In this work, the effectiveness of the grid refinement will be addressed through the comparison with the experimental observations just focusing on the prediction of the anchoring. Since the application of a certain amount of thickening on a diffusive flame front is theoretically wrong, all the simulations performed in the context of this study have been carried out with the aforementioned FI correction.

Investigated experimental conditions

The validation of the proposed numerical approach is based on the DLR experimental setup described in Saini et al. [13]. The optically accessible high-pressure combustion chamber at DLR (Fig. 1) is used to study the flame-holding behavior of a fuel jet in crossflow under different hydrogen contents. The rig is composed of three rectangular modules, the last one equipped with a 2 mm diameter hole from which the fuel is injected. The first two modules are necessary to ensure the formation of a well-developed boundary layer before mixing with the fuel jet. Detailed measurements such as PIV, OH-PLIF and OH* chemiluminescence are executed to retrieve information about the flow dynamics of the jet and the flame morphology, which will be used to validate the numerical approach.

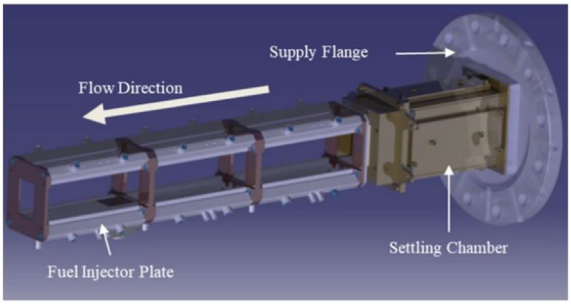

Fig. 1 – *Sketch of the test rig at DLR* [13].

With the operating pressure of the rig at 10 bar and the temperature of the oxidizer at 530 K, the tests are executed for two percentages of hydrogen in the fuel gas, according to Table 1. Despite the low velocities of the streams, the jet in cross flow velocity ratio and the momentum flux ratio are at values relevant for modern gas turbine injection systems.

Numerical setup

Computational domain and grid

From a numerical standpoint, in order to minimize the computational effort, only the last module of the flow channel shown in Fig. 2 is modelled. The impact of the not-included modules is taken into account by imposing a proper inlet crossflow boundary condition. A similar approach has been adopted for the fuel jet feeding line.

The computational mesh resolution plays a fundamental role in the ability of the simulation to correctly capture the flame anchoring location dealing with both premixed and diffusive combustion regimes. Two different mesh strategies have been adopted. The first one employs a static mesh with different resolutions along the domain. Fig. 2 shows a longitudinal and a transverse section of the grid where these differences can be visualized. In particular, four zones are defined. The finest resolution of 50 μm is applied inside a

Table 1 – Summary of the reference test conditions.

Quantity	Case 1	Case 2
H_2 (vol. %)	40	20
Operating Pressure	10 bar	
Oxidizer Temperature	530 K	
Cross Flow Velocity	1.47 m/s	
Fuel injection velocity	18.2	16.2
Jet crossflow velocity ratio	12.4	11.0
Jet crossflow density ratio	0.69	0.88
Momentum flux ratio	10.3	
Jet Reynolds number	14,350	16,340
Crossflow Reynolds number	16,400	

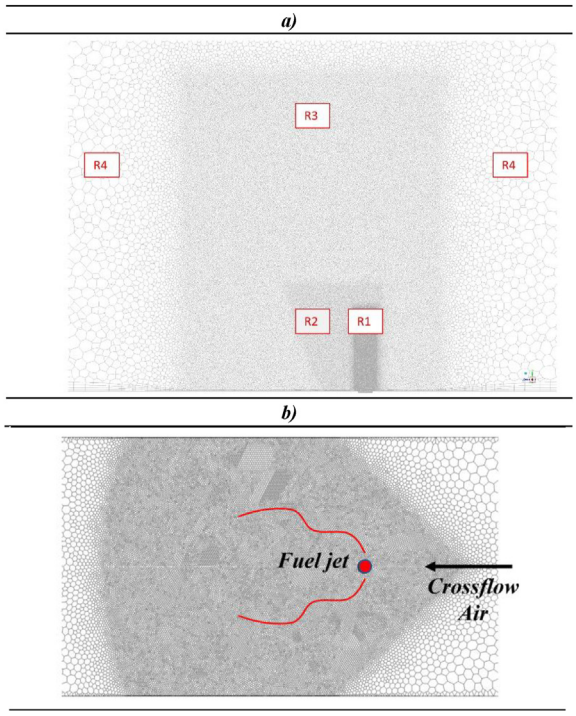

Fig. 2 – Computational static grid on (*a*) midplane longitudinal section with flow direction from right to left (*b*) and transverse plane with flow direction from left to right.

cylinder (R1 in Fig. 2) surrounding the fuel jet whose height is equal to 10 diameters. The second zone (R2), whose shape is designed also to capture the downstream recirculation zone of the flow, has a resolution of 100 μm.

Zone R3 has a height able to properly capture the maximum jet penetration: it has a mesh resolution of 150 μm. In all the other regions of the domain, both upstream and downstream of the fuel jet, the mesh is built with no additional prescriptions. The use of a FR treatment of the diffusive flame front is feasible thanks to the higher numerical stability of these flames which can be solved even with very coarse meshes [33]. However, in such cases, the presence of high strain rates (thus thin diffusive flames) is expected to lead to a misprediction of the extinction strain rate. Since a uniform finer grid would not be affordable from a computational perspective, a dynamic refinement on the flame front has been considered in order to overcome this modelling weakness.

The second strategy acting on top of the above-described static mesh is based on an Automatic Mesh Refinement (AMR) algorithm able to locally adapt the spatial discretization according to user-defined quantities. The mesh is dynamically adapted (with a maximum of two refinement levels) where the mixture fraction gradient is higher than a pre-defined threshold and only in the regions where $0.8 \bullet Z_{sto} < Z < 1.1 \bullet Z_{sto}$. A dedicated user-defined function is used to calculate the mixture fraction and its gradient according to the Bilger's definition. Fig. 3 shows an instantaneous contour plot of the mixture fraction with superimposed the corresponding grid. The application of the AMR algorithm leads the cell count from about 6 million of the static mesh up to 13 million polyhedral elements.

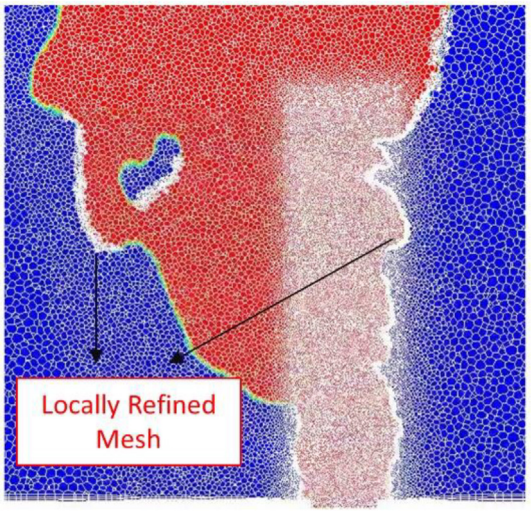

Fig. 3 – AMR application: the mesh is refined mainly in the region upstream of the jet. Contour plot: mixture fraction between 0 (blue) and the stoichiometric value (red). (For interpretation of the references to color in this figure legend, the reader is referred to the Web version of this article.)

Boundaries

Both the crossflow and the fuel inflow boundaries have been treated as a velocity inlet imposing a prescribed time average velocity profile derived from RANS simulations. The RANS simulations have been carried out including in the domain the whole length of the crossflow channel and the fuel feeding line, the velocities profiles have been extracted from such RANS simulations and imposed on the LES. Synthetic turbulence has been superimposed on the velocity profiles with an intensity respectively, of 10% and 5% for the crossflow and for the jetAll the walls are treated as adiabatic adopting a wall-function approach to model the boundary layer.

Chemistry treatment

Finite rate CFD combustion models with detailed chemistry can be challenging for industrial applications since they require the solution of individual species transport equations. In order to reduce the computational effort, detailed chemical schemes must be reduced to maintain only the most relevant reaction pathways, while preserving accuracy in the widest possible range of applicability. Regarding the latter aspect, the adoption of extremely reduced chemical mechanisms, even if optimized, it is not recommended since their performance cannot be reliable outside the optimization range. In the present work, a new skeletal mechanism able to handle blends of methane (as natural gas surrogate) and hydrogen at different volumetric percentages is firstly derived. The adopted strategy follows the most relevant reduction steps presented by Lu et al. [39,41] and Cazères et al. [42], leveraging the commercial code CHEMKIN-Pro [43]. The UCSD mechanism [44] is used as master chemical kinetic from which the reduced one is calculated. It consists of 57 species and 268 reactions with

hydrocarbon species up to C4, without the inclusion of the NOx chemistry set. A freely propagating flame is selected as canonical case to dynamically retrieve a comparison between the reduced mechanism with the original detailed mechanism. Details regarding the methodology and the setting employed to perform the chemical reduction are provided in the supplementary materials with an extensive validation of the skeletal mechanism. The resulted skeletal mechanism counts 26 species and 119 reactions. A stiff chemistry solver has been adopted to handle the runtime chemistry solution during the LES calculations. The use of such a chemistry solver allows the decoupling of the chemical timestep from the one of the fluid. In this way, the only constrain of the fluid timestep from the chemistry perspective is that it has to be lower than the diffusive timescale to provide an adequate reconstruction of the diffusive fluxes.

Sub-grid turbulence treatment, numerical schemes, and timestep

The Dynamic-Smagorinsky LES formulation, which allows the Cs constant to be locally determined during the calculation, is employed to model the unresolved scales of turbulence. The second-order upwind scheme is used for all the transport equations, but the momentum fluxes are resolved through a bounded central differencing scheme. The adopted time step size is such that the maximum convective Courant number is kept below the unity in all the simulated operating conditions. The temporal integration is carried out with an implicit second-order scheme. The time-averaged results shown in this work are collected after a sufficiently long washing-out phase with the simulation running for several Flow-Through Times (FTT) to be sure that a statistically consistent state is reached.

Results

Several LES simulations have been performed on the 20% and 40% H2 test points to investigate the FI-ATFM model predictivity. According to the experimental measurements of Saini et al. [13], the change in the H2 content is sufficient to observe a substantial change in the flame anchoring characteristics. This aspect offers the chance to validate the capacity of the numerical setup to predict the change in the flame morphology induced by the hydrogen addition. In the results discussions, firstly, a series of modelling setup investigations have been performed on the 40% H2 content test point to identify the best setup (best cost-accountancy compromise). Secondly, the identified setup has been tested also on the 20% H2 test point proving its effectiveness. A summary of all the simulations performed is reported in Table 2 and justified below.

Since the combustion regime is expected to be consistently dominated by the diffusive nature, the above-discussed issues in modelling the diffusive flame front must be carefully accounted for. As it has been already highlighted, the fact that the flame front thickening is neither correct nor effective with diffusive flames, rises the need to assess the effect of the grid discretization on the flame front prediction. In this work, the use of a flame front AMR has been investigated to understand the contribution of a finer flame front discretization wherever the mixing field thins the front. For this reason, as reported in Table 2, a couple of simulations have been performed in order to investigate this aspect. Another aspect on which this work aims to shed light on is the role of the thickening. In the ATFM the parameter N_{Thick} controls the number of points to be placed within the laminar flame front determining the amount of thickening introduced by the model. Even if in the FI-ATFM the thickening is applied only on the premixed front, the need for thickening in such a complex multi-regime flame front remains a topic to be further investigated. This justifies the second pair of simulations that have been performed.

Table 2 – Summary of the performed simulations and investigated setup.

	$N_{Thick} = 1$, FR, no AMR	$N_{Thick} = 1$, FR, with AMR	$N_{Thick} = 9$, no AMR	$N_{Thick} = 9$, with AMR
40% H2	X	X	X	X
20% H2	-	-	X	-

The results will be shown introducing firstly the flow field validation in reactive conditions. This comparison will be presented only for the cases without the AMR to prove that the static mesh, on which the AMR has been applied, is able to provide a satisfactory reconstruction of the flow field. Indeed, the local AMR slightly affects the velocity field only through a more accurate reconstruction of the flame front.

Reactive velocity field characterization

Fig. 4 compares the time average reactive velocity profiles with the time average experimental PIV measurements; in the same plot both the RMS of the simulation and the measurements are reported. The correspondence of the numerical prediction in the region near the jet (x = 2 mm–8mm) with the measurements is very good for both cases 40% H2 and 20% H2; the velocity peak due to the jet penetration is well captured in terms of location, mean velocity and RMS by the simulation. Moving downstream the jet, the prediction seems to get worsen for the 40% H2 case (F9-b). There, the low reliability of the experimental data must be highlighted: in fact, the soot scattering prevents the correct seed parcels velocity calculations [13].

The experimental results of Saini et al. [13] show that jet penetration is not strongly influenced by the H2 content if the momentum ratio is kept constant. Observing the red dashed line in Fig. 4, the numerical prediction of the centreline velocity trajectory of the jet can be reconstructed and, comparing the two cases at 20% and 40% H2, no significant differences in the trajectory prediction are observed, consistent with the aforementioned experimental finding. It is worth noting that the 20% and 40% H2 cases strongly differ on the flame anchoring position, thus the flow re-laminarization due to the presence of the flame does not significantly affect the penetration trajectory in this (highly confined) jet flame in crossflow.

As will be pointed out later in this work, the velocity flow field and the corresponding flame strain have a high impact on the flame anchoring on the windward side (WS). The solved

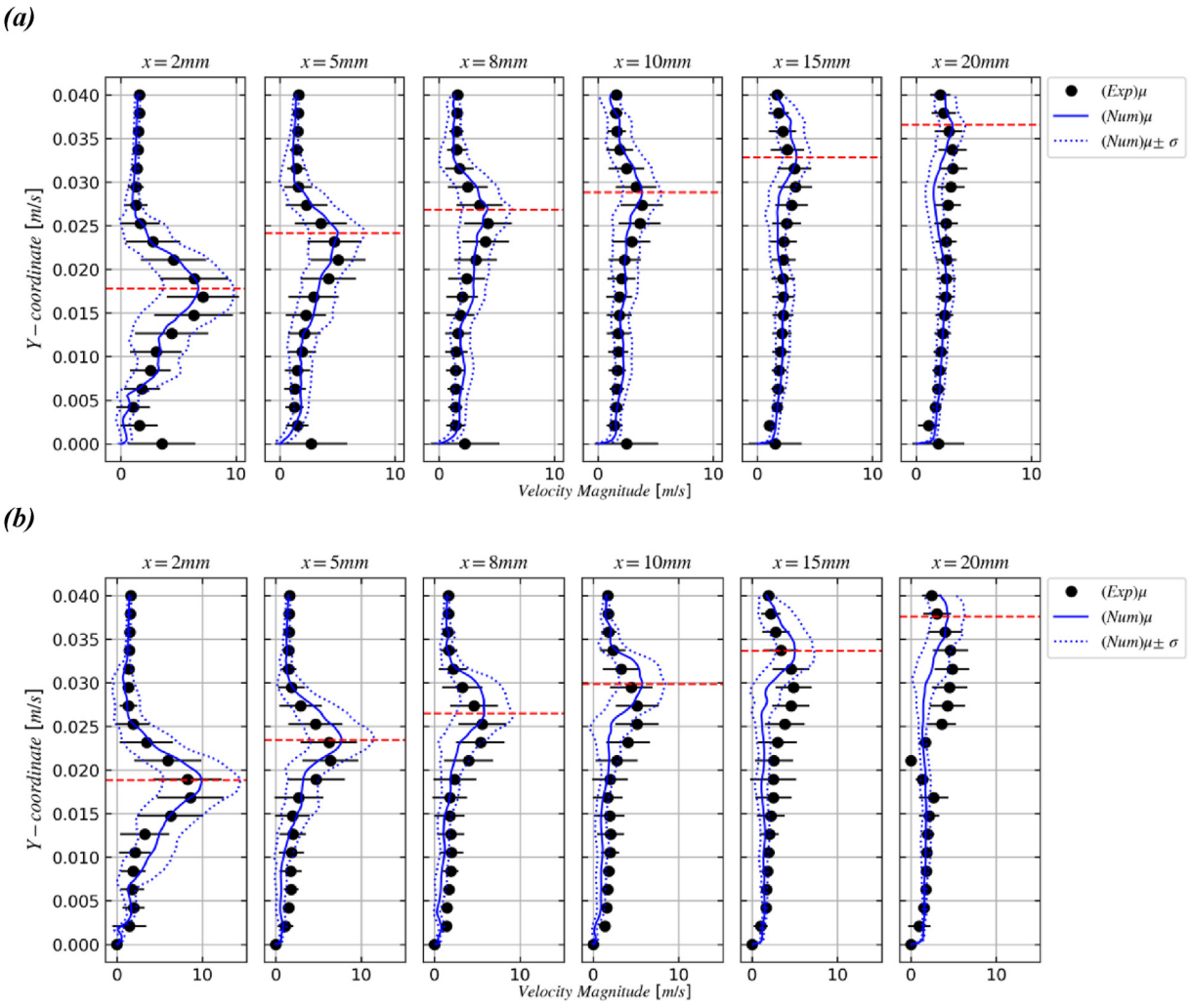

Fig. 4 – Time-averaged velocity magnitude profiles comparison for different axial locations. Numerical time average velocity magnitude (continuous lines). Experimental time average velocity magnitude (points). 1 σ confidence interval of the numerical prediction (dotted lines), 1 σ confidence interval of the experimental measurements (error bar). (*a*) 20% H2 case without AMR, (*b*) 40% H2 case without AMR. Horizontal dashed red lines represent the position of the numerical maximum of velocity magnitude, thus outlining the predicted jet centreline trajectory. (For interpretation of the references to color in this figure legend, the reader is referred to the Web version of this article.)

aerodynamic flame strain is defined in Eq. (6) where n is the normal vector to the flame front that is assumed to be located on the stochiometric iso-surface. The solved strain rate will be called simply strain rate in the next paragraph.

$$\alpha = \nabla u - n(\nabla u \bullet n) \tag{6}$$

Flame morphology 40% H2

Numerical predictions comparison

For this 40% H2 test point four LES simulations have been performed. The first pair of simulations are carried out with $N_{Thick} = 1$ enabling and disabling the AMR. Especially for the AMR case, the finer mesh resolution around the above-reported mixture fraction ratio range, leads to a thickening factor close to the unity in the entire flame anchoring location and the combustion model closure is *de-facto* the finite-rate (FR) one. The second pair of simulations are run with $N_{Thick} = 9$. Also in this case, both the meshing strategies have been tested.

In Fig. 5 the instantaneous and time-averaged numerical predictions, of all the cases, are compared with the experimental measurements. The first finding of the comparison among the cases is that, independently of the adopted mesh strategies, the use of $N_{Thick} = 1$ leads the flame front to be quickly and permanently extinguished from the WS, contrary to the experimental observations. Focusing more on the two $N_{Thick} = 1$ cases comparison, the only difference is that the flame front upstream of the fuel jet has been kept longer when the AMR is used. This could suggest a slight effectiveness of the AMR in improving the resolution of the flame front. These results led to the decision not to collect statistics for the two

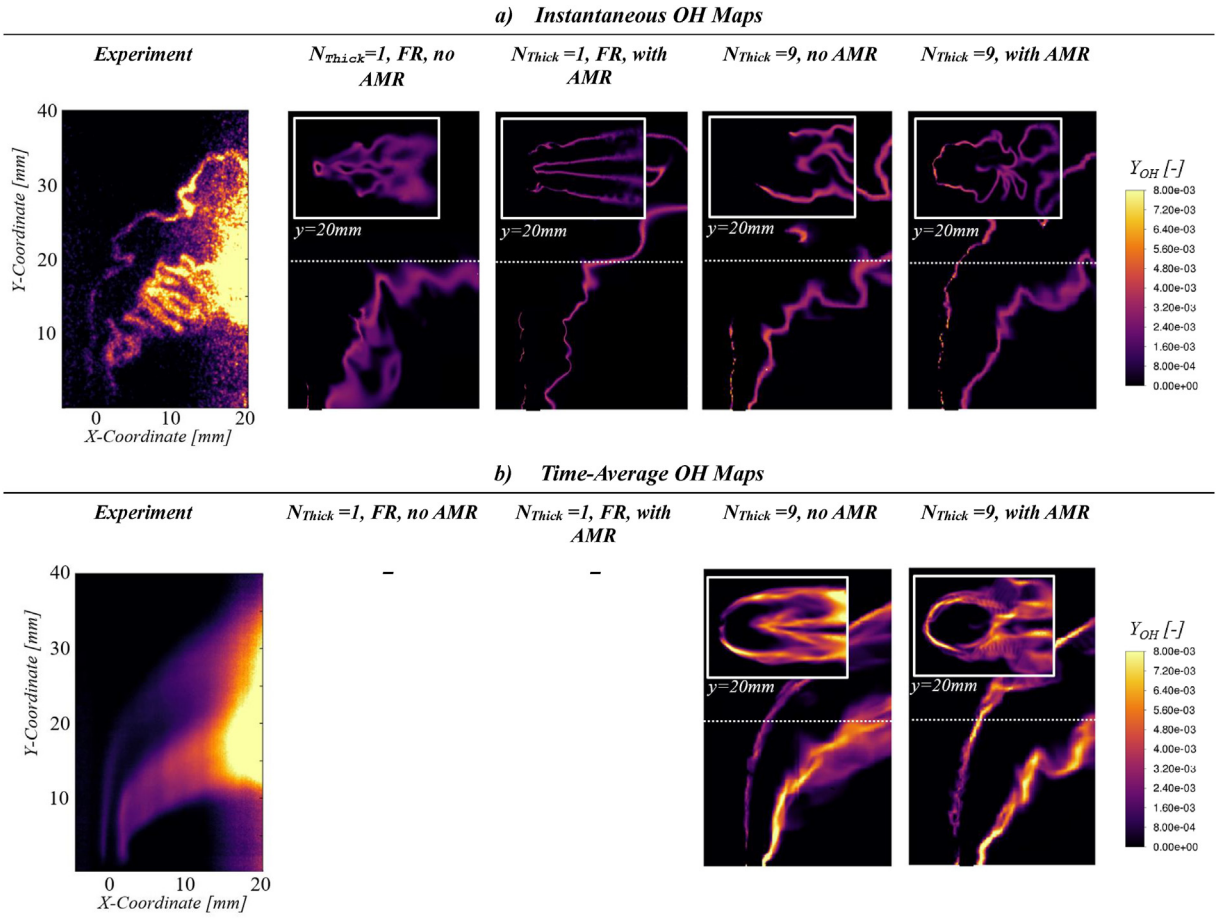

Fig. 5 – *a)* Instantaneous Y_{OH} contour and OH-PLIF (from Saini et al. [13]); *b)* time-averaged experimental OH-PLIF (from Saini et al. [13]) and numerical time-averaged Y_{OH} contour plots on the longitudinal plane and on the $y = 20$ *mm* plane.

$N_{Thick} = 1$ simulations. On the other side, when the thickening factor is increased by increasing N_{Thick}, the model accurately predicts the flame front anchoring also on the windward region providing good agreement with the experimental OH-PLIF data. No significant discrepancy was observed while comparing the two time-averaged numerical results with $N_{Thick} = 9$, except for a slight difference in the mean Y_{OH} value. From this qualitative comparison between the cases, it can be concluded that the most challenging and crucial part of the flame front to be numerically reconstructed is the anchoring on the WS. Basing the comparison among the cases on this aspect, the use of the AMR has not been found crucial, whereas the premixed front thickening has turned out to be essential ($N_{Thick} > 1$).

In order to provide some explanations of the numerical reasons that make the anchoring prediction on the WS so challenging, the impact of the mixing field on the flame front will be presented in the next paragraph.

Mixing impact on the flame and combustion regime

Fig. 6 reports, on the longitudinal (Fig. 6-a), and transversal (Fig. 6-b) plane, the Z_{sto} ($Z_{sto} = 0.053$) isoline together with other 2 Z isolines taken respectively on the lean and rich side. The spacing between the Z isolines in Fig. 6 suggests that there is a significant difference in the Z gradient around the fuel jet and this has an impact on the time scales of the mixing (τ_T). In a stratified or diffusive flame front, the combustion regime is controlled by the Damkholer number (Da) that can be evaluated by the ratio between the mixing and the chemical timescale ($Da = \tau_T/\tau_c$). The very different spacing between the Z isolines reported in Fig. 6 suggests that the Da is subjected to a strong variation around the fuel jet. LS of the jet is characterized by very low Z gradient, thus, the fast chemistry assumption is reasonable in this region due to the low τ_T. Such flame front peculiarity makes modelling this part of the flame front easier even without additional thickening. On the contrary, the flame front on the WS is subjected to an intense Z gradient that makes τ_T comparable τ_c. In these conditions the finite rate chemistry assumes a primary role and the flame front becomes very thin leading to an intensification of gradients of the species across the cells. This flame front thinning enhances the numerical diffusion and raises difficulties in the prediction of the flame extinction limit. As a result, the prediction of the flame anchoring on the WS is particularly challenging to be captured from the modelling perspective.

In the same Fig. 6 the $\dot{\omega}_{fuel}FI$ contour plot is shown. Leaving aside the FI value and focusing firstly only on the intensity of the colour (regardless of whether it is blue or red), Fig. 6 shows

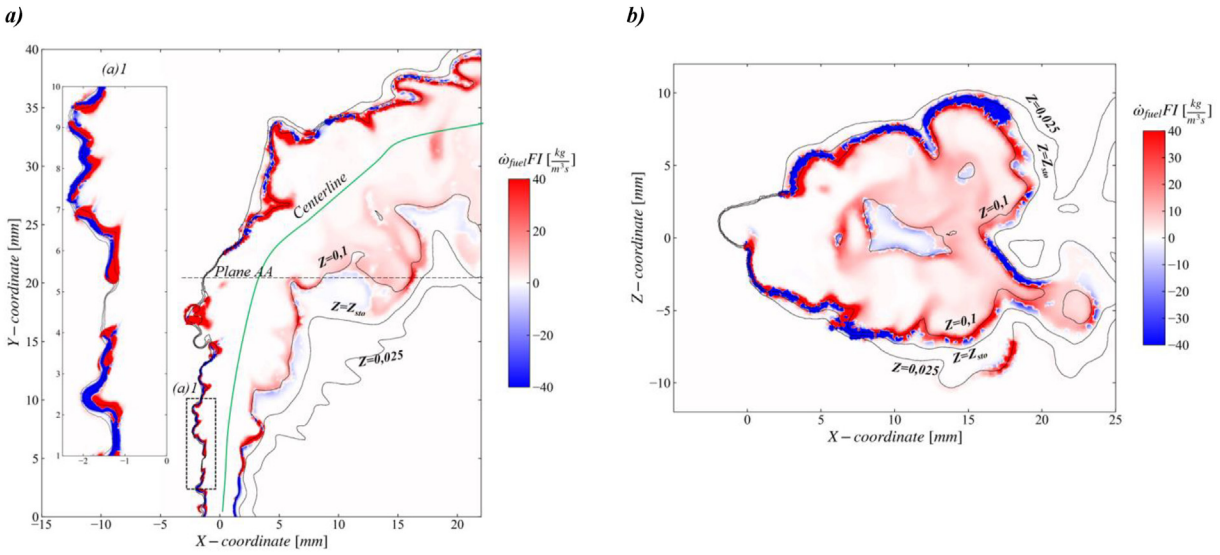

Fig. 6 – *(a)* Numerical instantaneous contour of $\dot{\omega}_{fuel}FI$ for the 40% H2 case with AMR on XY longitudianl plane, the green line identifying the predicted Jet centerline trajectory of the mixing field; (a)1 magnification of the flame front on the windward side; *(b)* section on the A-A plane of the domain showing $\dot{\omega}_{fuel}FI$ on the XZ transversal plane. Negative values identify zones where the combustion process takes place in a diffusive regime while positive values are regions where the combustion is premixed. (For interpretation of the references to color in this figure legend, the reader is referred to the Web version of this article.)

that the fuel consumption of the flame front is strongly influenced by the mixing intensity. Wherever the Z gradient is more intense the fuel consumption is locally higher, in contrast on the LS, the lower Z gradient makes the fuel consumption diminish. This behavior is the typical diffusive flame front response with respect to stretch. Thus, as in a diffusive flame, in this JICF flame, the mixing field affects the fuel consumption making the flame front on the Windward Side (WS) very different from the one on the Leeward Side (LS).

All these considerations are based on the theory of perfectly diffusive flame fronts, however, up to this point, it is still unclear what is the dominant combustion regime in the JICF flame.

The FI parameter allows the distinction of the premixed from the diffusive combustion regime. Even if the FI is defined all over the domain, it is meaningful to look at this quantity only where the combustion occurs. According to this, an effective way to identify these regions is to filter the FI with the local fuel consumption considering the products $\dot{\omega}_{fuel}FI$:

$$\dot{\omega}_{fuel}FI = -FI(\dot{\omega}_{CH4} + \dot{\omega}_{H2}) \tag{7}$$

The $\dot{\omega}_{fuel}FI$ contour, shown in Fig. 6, suggests that even if the flame develops on an intense mixture fraction gradient it is far from being completely diffusive. In particular, the premixed regime becomes dominant increasing the y coordinate due to the higher mixing between the air and the fuel. Nevertheless, focusing on the early part of the LS, the magnification of the flame front in Fig. 6-a(1) reveals that the premixed mode is intimately mixed with the diffusive one.

The role of the premixed front and of its thickening

Trying to investigate the role of the thickening in the complex multi-regime flame front, it is useful to introduce a coordinate transformation. The visualization of the 3D flame front that envelops the JICF has been made easier by a remap of the cartesian (x, y, z) coordinates, into a curvilinear cylindrical reference system (r, θ, s): s represents the curvilinear abscissa taken on the mixing jet centerline trajectory, r, and θ the cylindrical coordinates computed respect to the centerline. In this way, r always represents the distance of a certain point of the domain from the centerline. The mixing jet centerline trajectory is shown in Fig. 7-a and is computed as the locus of points which has maximum Z increasing the y coordinate. In Fig. 7 the $\dot{\omega}_{fuel}FI$ scatterplot is shown on the remapped stochiometric iso-surface with respect to the (θ, s) coordinates, which are orientated such that $\theta = 0$ is on the WS of the jet and $\pm\pi$ identify the LS. The differences in the density of the points in Fig. 7 are due to the mesh sizing non-uniformity that is statically and dynamically refined decreasing the s coordinate due to the increasing Z gradient.

Focusing on the $N_{Thick} = 9$ cases (Fig. 7-a), in the early fuel-jet shear layer (s < 0.020 m) the majority of the windward side of the jet is diffusive. In that region, several local flame front extinctions can be identified ($\dot{\omega}_{fuel}FI = 0$). The edges of these extinction zones are almost always surrounded by a premixed flame front; indeed, the propagation of the flame front in the direction tangential to the Z iso-surface must be premixed according to the triple flame investigations of Im et al. [45]. As a result, wherever the extinction is surrounded by a non-premixed region it means that the flame is not currently propagating along the Z_{sto} isosurface shown. Moving away from $\theta = 0$, the fuel consumption gets progressively premixed before finally being lost on the LS. The same considerations can be done also looking at the transversal section of Fig. 6-a where the fuel consumption on the LS is shifted from the stochiometric isoline towards richer mixtures.

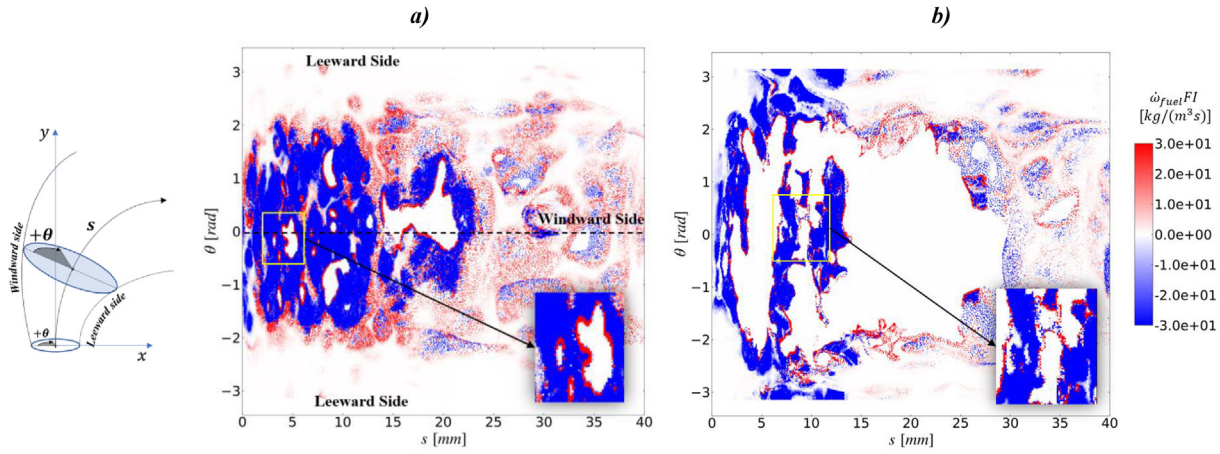

Fig. 7 – Scatterplot showing the grid nodes extracted on the instantaneous Z_{sto} value. Negative values $\dot{\omega}_{fuel}FI$ identify a diffusive fuel consumption, whereas positive values identify premixed fuel consumption; *a)* 40%H2 case with AMR and $N_{Thick} = 9$; *b)* 40%H2 case with AMR and $N_{Thick} = 1$.

To understand the mechanism that leads to the flame front extinction on the WS for the FR cases, a time instant in which the flame is still present on the WS has been analyzed in Fig. 7-b. Beforehand, the only modelling difference between the two AMR cases is the treatment of the premixed front, thus the difference in the results must be fully ascribed to this. Comparing the $\dot{\omega}_{fuel}FI$ for the two cases in Fig. 7-a and Fig. 7-b, it emerges that the FR case has a flame front that is almost completely diffusive: the premixed regime is observed only for a few points on the flame front edges. This suggests that the employed setting of the ATFM (i.e., the value of N_{Thick}), is not able to predict a self-sustained premixed front: despite the extremely fine mesh, the low number of points placed in the flame thickness ($N_{Thick} = 1$) is not able to fully resolve the chemistry scales and, consequently, to reproduce the correct fuel consumption speed which is the crucial aspect to be captured in such regime. As expected, the FR model is not appropriate for the description of the premixed flame front, nevertheless, the diffusive flame front can be modelled with the same FR approach. This demonstrates the very different modelling requirements that the two combustion regimes have, confirming what has been stated in the modelling section. Moreover, the analysis shows the essential role of mutual interaction between the diffusive and the premixed flame front, from this it emerges that the diffusive flame front cannot propagate without the premixed one. The appropriate modelling of the premixed part must consider a certain amount of thickening, and this justifies the effectiveness of the FI-ATFM.

Flame morphology 20%H2 case

Flame front prediction

The test condition with 20% vol. H_2 in the fuel blend is simulated without the AMR strategy with $N_{Thick} = 9$ points within the flame thickness. This setting represents the best accuracy-computational cost compromise, according to the findings discussed in the previous paragraph. Fig. 8-a shows the sequence of Y_{OH} contour right after the LES start from the RANS simulation: it can be seen that the flame front is completely lost after only 2.56 ms in the windward region. On the contrary, the anchoring on the LS is kept during this transitory phase. Looking at the time-averaged results, shown in Fig. 8-b, the total absence of the flame on the WS is confirmed. Both the experiment and prediction are in good agreement on this. The numerical simulation shows that the flame front remains anchored on the LS, thus, confirming the experimental evidence and proving the capability of the model to provide a qualitative reconstruction of the flame topology. However, the near-wall flame brush is overestimated just behind the fuel jet exit. The inclusion of the wall heat losses would have contributed to improving the prediction in this region. Nevertheless, the heat loss effect is expected to be localized only in this region because the flame is everywhere detached from the walls.

In the experimental map, the flame is slightly detached from the wall due to the near-wall heat losses. Despite that, the presence of a weak OH trace on the WS has been detected by the experimental measurements. In the numerical prediction, the flame front is attached to the wall but after barely 1 mm the numerical prediction found a good accordance with the experimental data on the WS predicting the flame presence.

Extinction mechanism on the WS

Trying to go deeper into the predicted extinction mechanism on the WS, two scatterplots on the remapped Z_{sto} surface are shown in Fig. 9. Observing the flame anchoring and the combustion regime (Fig. 9-a), the anchoring on the WS is sharply lost nearby $s = 5mm$. Increasing $s > 5mm$, the fuel consumption on the WS gets lost and the flame stabilizes on the LS in the recirculation region behind the jet, becoming completely premixed. Focusing on the extinction region on the WS, the magnification in Fig. 9-a shows that the flame

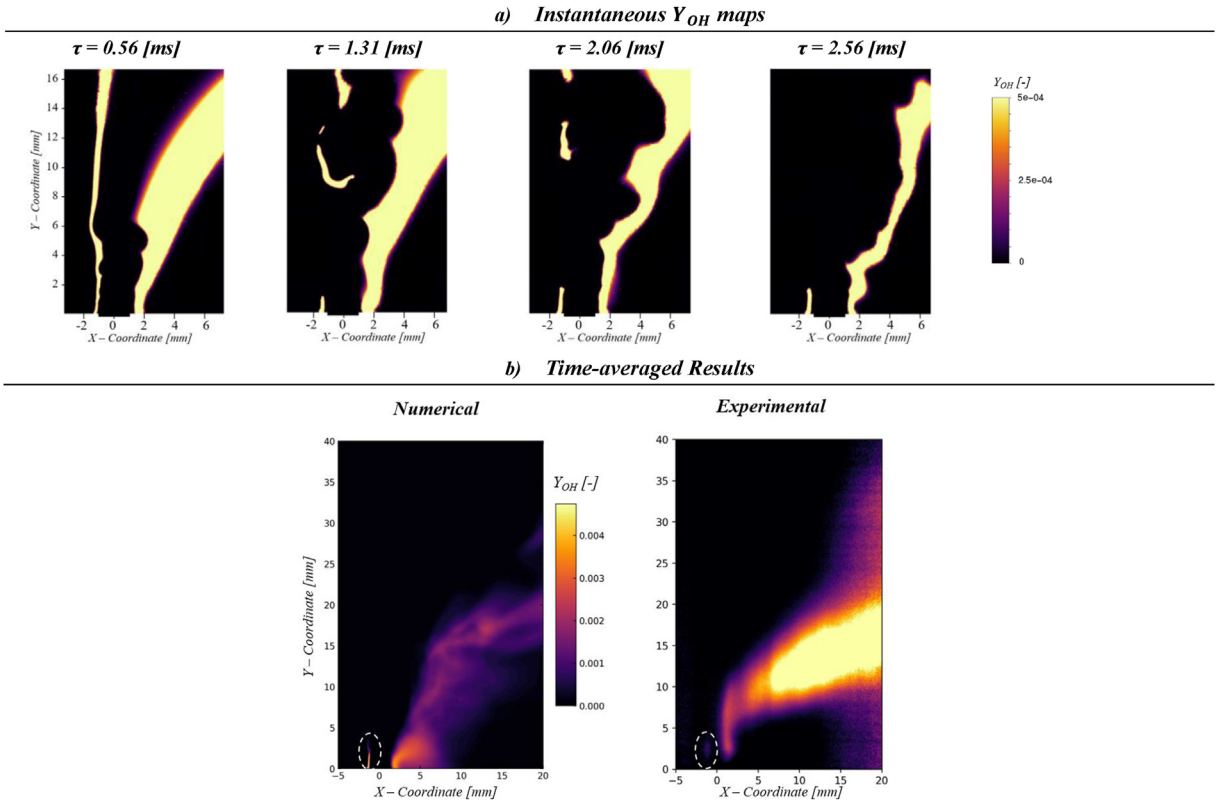

Fig. 8 – *a)* Y_{OH} instantaneous contour of the transitory phase from the initial RANS solution. *b)* Time-averaged results of OH mass fraction compared with the corresponding time-averaged experimental OH-PLIF [13]. In both figures the presence of Y_{OH} on the windward side has been highlighted.

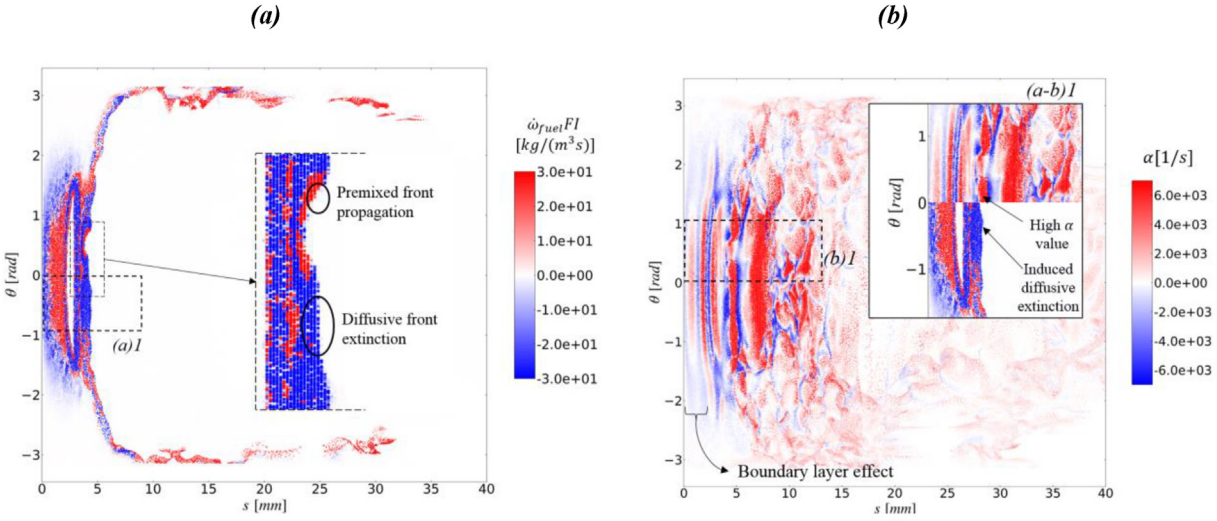

Fig. 9 – Scatterplot showing the grid nodes extracted on the instantaneous Z_{sto} surface. The nodes have been reported according to the θ, s coordinates; *a)* the colormap represents the $\dot{\omega}_{fuel}FI$; *b)* the colormap represents the solved strain rate acting on the Z_{sto} surface. In the magnification *(a–b)1* detail related to both figures (*(a)1* for figure *(a)* and *(b)1* for figure *(b)*) has been flanked each other in order to facilitate the comparison between the two fields.

front ends up mostly with the diffusive regime. These diffusive extinctions occur when the model is not able to sustain the diffusive front, thus when the solved strain rate exceeds the predicted extinction limits. Indeed, the decrease in the H2 content leads to a strong reduction in the diffusive extinction resistance (supplementary materials), which finally results in a higher flame propensity to be extinguished in the high strain rate regions.

To highlight the strain rate effect on the flame front, in Fig. 9-b the strain rate acting on the front itself has been

reported on the Z_{sto} surface. The Z_{sto} surface, and the flame front with that, is periodically wrinkled by the passage of the Kelvin Helmholtz instabilities. Their effect on the strain rate field can be identified by the circumferential strain bands, that alternately assume positive (red) and negative (blue) values on the WS. The boundary layer attenuates the strain rate for $s < 2mm$ and allows the flame to be locally stabilized in this region as confirmed by Fig. 9-a. Increasing s in Fig. 9-b, the peak of positive strain rate increases sharply on the WS, and it leads to the circumferential extinctions shown in Fig. 9-a around $s = 2.5mm$ which is extended in the angular direction for $-1.5 < \theta < 1.5$. By a further increase of the curvilinear coordinate ($s < 2mm$), an extended flame front extinction all over the WS, induced by the rising positive strain rate levels, can be observed. As evidence of that, in the magnification shown in Fig. 9-b, the role of the high compressive strain rate on extinction can be recognised. Indeed, the peak of the positive compressive strain rate is aligned with the diffusive extinction proving the strong local correlation between the two phenomena. In conclusion, for this 20% H2 case, the flame front cannot be sustained on the windward side due to the combination of two main effects: firstly, the front is highly prone to diffusive extinctions, and secondly, the premixed flame front propagation is not sufficiently fast to recover the flame once the extinction occurs. The role of the premixed flame front must not be neglected; indeed, local extinctions have been observed also on the 40% H2, however in this case the propagation speed is enough to restore the front once the extinction occurs.

In any case, it can be stated that the adopted numerical process is able to reproduce the physics of the flame anchoring, demonstrating a robust generality against the range of fuel compositions here investigated.

Conclusions

In this work, a set of numerical investigations of a JICF flame have been conducted to validate the FI-based ATFM formulation for the treatment of multi-regime turbulent combustion. In this context, a novel CH4/H2 skeletal reaction mechanism has been derived, and its validation has been supported by a wide range of operating conditions and flame configurations.

In the DLR experimental campaign on the JICF [13], the change in the H2 content of the fuel mixture from 20% to 40% was observed to substantially change the flame topology and stabilization process. Trying to numerically reproduce the flame anchoring topology observed in the experiments, high-fidelity simulations have been performed to explore the accuracy of the FI-based ATFM. Starting from the 40% H2 case, two levels of thickening have been adopted to better understand the impact on the flame extinction mechanism. Results show that the use of higher N_{Thick}, thus the increase of F_{max} of the premixed front, is unavoidable to capture the flame anchor on the windward side of the flame. Indeed, despite the two combustion regimes being intimately mixed, the flame front propagation along the mixing layer must be premixed and so it requires some thickening to be properly solved. On the opposite, when the flame front is diffusive the thickening must be suppressed to avoid altering the reactivity. The use of the AMR, on the 40% H2 test point, has not provided substantial solution improvements, this has demonstrated that the moderate discrepancy from the experimental results is not due to an inappropriate diffusive flame front discretization. Decreasing the amount of H2, the change in the flame stabilization region has been correctly predicted by the model. In this low H2 content case, the role of the compressive strain rate inducing local flame front extinctions on the windward side has been underlined. The fact that flame anchorage has been no longer predicted on the windward side is due to the occurrence of these extinctions combined with the lower premixed flame propagation speed. In conclusion, this work proves the effectiveness of the FI-ATFM model for the application's context where the combustion is expected to be locally non-premixed.

Declaration of Competing Interest

The authors declare that they have no known competing financial interests or personal relationships that could have appeared to influence the work reported in this paper.

Acknowledgements

This project has received funding from the European Research Council (ERC) under the European Union's Horizon 2020 research and innovation program (Grant agreement No. 682383).

Appendix A. Supplementary data

Supplementary data to this article can be found online at https://doi.org/10.1016/j.ijhydene.2023.05.210.

REFERENCES

[1] Stiehl B, Otero M, Genova T, Worbington T, Reyes J, Martin S, Velez C, Ahmed K. Simulation of premixed and partially premixed jet-in-crossflow flames at high pressure. J Eng Gas Turbines Power 2021;143:1–7. https://doi.org/10.1115/1.4049703.

[2] Füri M, Papas P, Raïs RM, Monkewitz PA. The effect of flame position on the kelvin-helmholtz instability in non-premixed jet flames. Proc Combust Inst 2002;29:1653–61. https://doi.org/10.1016/s1540-7489(02)80203-6.

[3] Hasselbrink EF, Mungal MG. Transverse jets and jet flames. Part 1. Scaling laws for strong transverse jets. J Fluid Mech 2001;443:1–25. https://doi.org/10.1017/S0022112001005146.

[4] Frich T, Roshko A. Vortical structure in the wake of a transverse jet. J. Fluid Mech. Mech. 1994;279.

[5] Kelso RM, Lim TT, Perry AE. An experimental study of round jets in cross-flow. J Fluid Mech 1996;306:111–44. https://doi.org/10.1017/S0022112096001255.

[6] Karagozian AR. Transverse jets and their control. Prog Energy Combust Sci 2010;36:531–53. https://doi.org/10.1016/j.pecs.2010.01.001.

[7] Meloni R, Cerutti M, Zucca A, Mazzoni M. Numerical modelling of NOx emissions and flame stabilization mechanisms in gas turbine burners operating with hydrogen and hydrogen-methane blends. 2020. https://doi.org/10.1115/GT2020-15432.
[8] Meloni R, Gori S, Andreini A, Nassini PC. CO emission modeling in a heavy duty annular combustor operating with natural gas. J Eng Gas Turbines Power 2021;144. https://doi.org/10.1115/1.4052028.
[9] Meloni R, Nassini PC, Andreini A. Model development for the simulation of the hydrogen addition effect onto the NOx emission of an industrial combustor. Fuel 2022;328:125278. https://doi.org/10.1016/j.fuel.2022.125278.
[10] Hasselbrink E, Mungal MG. Non-premixed methane transverse jet flames. 27th Symp. Combust. 1998:1167–73.
[11] Han D, Mungal MG. Direct measurement of entrainment in reacting/nonreacting turbulent jets. Combust Flame 2001;124:370–86. https://doi.org/10.1016/S0010-2180(00)00211-X.
[12] Steinberg AM, Sadanandan R, Demb C, Kutne P, Meier W. Structure and stabilization of hydrogen jet flames in cross-flows. Proc Combust Inst 2013;34:1499–507. https://doi.org/10.1016/j.proci.2012.06.026.
[13] Saini P, Chterev I, Pareja J, Aigner M, Boxx I. Effects of hydrogen-enrichment on flame-holding of natural gas jet flames in crossflow at elevated temperature and pressure, flow. Turbul. Combust. 2021;107:219–43. https://doi.org/10.1007/s10494-020-00230-1.
[14] Saini P, Chterev I, Pareja J, Aigner M, Boxx I. Effect of pressure on hydrogen enriched natural gas jet flames in crossflow, flow. Turbul. Combust. 2020;105:787–806. https://doi.org/10.1007/s10494-020-00148-8.
[15] Grout RW, Gruber A, Yoo CS, Chen JH. Direct numerical simulation of flame stabilization downstream of a transverse fuel jet in cross-flow. Proc Combust Inst 2011;33:1629–37. https://doi.org/10.1016/j.proci.2010.06.013.
[16] Kolla H, Grout RW, Gruber A, Chen JH. Mechanisms of flame stabilization and blowout in a reacting turbulent hydrogen jet in cross-flow. Combust Flame 2012;159:2755–66. https://doi.org/10.1016/j.combustflame.2012.01.012.
[17] Galeazzo FCC, Donnert G, Habisreuther P, Zarzalis N, Valdes RJ, Krebs W. Measurement and simulation of turbulent mixing in a jet in crossflow. J Eng Gas Turbines Power 2011;133:1–10. https://doi.org/10.1115/1.4002319.
[18] Chan WL, Kolla H, Chen JH, Ihme M. Assessment of model assumptions and budget terms of the unsteady flamelet equations for a turbulent reacting jet-in-cross-flow. Combust Flame 2014;161:2601–13. https://doi.org/10.1016/j.combustflame.2014.04.007.
[19] Ramaekers WJS, Albrecht BA, van Oijen JA, de Goey LPH, Eggels RLG. The application of flamelet generated manifolds in partially-premixed flames. 2005. p. 1–5.
[20] De Swart JAM. Modeling and analysis of flame stretch and preferential diffusion in premixed flames. 2009. https://doi.org/10.6100/IR651971.
[21] De Swart JAM, Bastiaans RJM, Van Oijen JA, De Goey LPH, Cant RS. Inclusion of preferential diffusion in simulations of premixed combustion of hydrogen/methane mixtures with flamelet generated manifolds, Flow. Turbul. Combust. 2010;85:473–511. https://doi.org/10.1007/s10494-010-9279-y.
[22] Donini A, Bastiaans RJM, Van Oijen JA, De Goey LPH. Differential diffusion effects inclusion with flamelet generated manifold for the modeling of stratified premixed cooled flames. Proc Combust Inst 2015;35:831–7. https://doi.org/10.1016/j.proci.2014.06.050.
[23] van Oijen JA, Donini A, Bastiaans RJM, ten Thije Boonkkamp JHM, de Goey LPH. State-of-the-art in premixed combustion modeling using flamelet generated manifolds. Prog Energy Combust Sci 2016;57:30–74. https://doi.org/10.1016/j.pecs.2016.07.001.
[24] Luo Y, Ferraro F, Breicher A, Bottler H, Dreizler A, Geyer D, Hasse C, Scholtissek A. A novel flamelet manifold parametrization approach for lean CH4-H2-air flame. Int J Hydrogen Energy 2022:618–9. https://doi.org/10.1016/j.ijhydene.2022.09.233.
[25] Wen X, Dressler L, Dreizler A, Sadiki A, Janicka J, Hasse C. Flamelet LES of turbulent premixed/stratified flames with H2 addition. Combust Flame 2021;230:111428. https://doi.org/10.1016/j.combustflame.2021.111428.
[26] Verhoeven LM, Ramaekers WJS, van Oijen JA, De Goey LPH. Modeling non-premixed laminar co-flow flames using flamelet-generated manifolds. Combust Flame 2012;159:230–41. https://doi.org/10.1016/j.combustflame.2011.07.011.
[27] Knudsen E, Pitsch H. Capabilities and limitations of multi-regime flamelet combustion models. Combust Flame 2012;159:242–64. https://doi.org/10.1016/j.combustflame.2011.05.025.
[28] Rosenberg DA, Allison PM, Driscoll JF. Flame index and its statistical properties measured to understand partially premixed turbulent combustion. Combust Flame 2015;162:2808–22. https://doi.org/10.1016/j.combustflame.2015.04.007.
[29] Yadav R, De A, Jain S. A hybrid flamelet generated manifold model for modeling partially. 2017. p. 1–10.
[30] Colin O, Ducros F, Veynante D, Poinsot T. A thickened flame model for large eddy simulations of turbulent premixed combustion. Phys Fluids 2000;12:1843–63. https://doi.org/10.1063/1.870436.
[31] Legier JP, Poinsot T, Veynante D. Dynamically thickened flame LES model for premixed and non-premixed turbulent combustion. Proc. Summer Program, Cent. Turbul. Res. 2000:157–68.
[32] De Luca G. Development of a dynamic LES model for turbulent diffusion flames Thèse de doctorat. 2021.
[33] Cuenot B, Shum-Kivan F, Blanchard S. The thickened flame approach for non-premixed combustion: principles and implications for turbulent combustion modeling. Combust Flame 2021:111702. https://doi.org/10.1016/j.combustflame.2021.111702.
[34] Aniello A, Laera D, Marragou S, Magnes H, Selle L, Schuller T, Poinsot T. Experimental and numerical investigation of two flame stabilization regimes observed in a dual swirl H2-air coaxial injector. Combust Flame 2023;249:112595. https://doi.org/10.1016/j.combustflame.2022.112595.
[35] Laera D, Agostinelli PW, Selle L, Cazères Q, Oztarlik G, Schuller T, Gicquel L, Poinsot T. Stabilization mechanisms of CH4 premixed swirled flame enriched with a non-premixed hydrogen injection. Proc Combust Inst 2021;38:6355–63. https://doi.org/10.1016/j.proci.2020.06.378.
[36] Burke SP, Schumann TEW. Diffusion flames. Proc. Symp. Combust. 1928;1–2:2–11. https://doi.org/10.1016/S1062-2888(65)80003-X.
[37] Wang H, Hawkes ER, Chen JH. A direct numerical simulation study of flame structure and stabilization of an experimental high Ka CH4/air premixed jet flame. Combust Flame 2017;180:110–23. https://doi.org/10.1016/j.combustflame.2017.02.022.
[38] Im HG, Chen JH. Preferential diffusion effects on the burning rate of interacting turbulent premixed hydrogen-air flames. Combust Flame 2002;131:246–58. https://doi.org/10.1016/S0010-2180(02)00405-4.
[39] Franzelli BG. Impact of the chemical description on direct numerical simulations and large eddy simulations of

turbulent combustion in industrial aero-engines, PhD.. 2011. p. 270.
[40] Durand L, Polifke W. Implementation of the thickened flame model for large Eddy simulation of turbulent premixed combustion in a commercial solver. Proc. ASME Turbo Expo 2007;2:869–78. https://doi.org/10.1115/GT2007-28188.
[41] Lu T, Law CK. Toward accommodating realistic fuel chemistry in large-scale computations. Prog Energy Combust Sci 2009;35:192–215. https://doi.org/10.1016/j.pecs.2008.10.002.
[42] Cazères Q, Pepiot P, Riber E, Cuenot B. A fully automatic procedure for the analytical reduction of chemical kinetics mechanisms for Computational Fluid Dynamics applications. Fuel 2021;303. https://doi.org/10.1016/j.fuel.2021.121247.
[43] Chemkin-Pro, Reaction Design Inc., San Diego, California, ([n.d.]).
[44] Chemical-kinetic mechanisms for combustion applications, san diego mechanism web page, mechanical and aerospace engineering (combustion research), university of California at san diego. http://combustion.ucsd.edu; 2014 [n.d.].
[45] Im HG, Chen JH. Structure and propagation of triple flames in partially premixed hydrogen-air mixtures. Combust Flame 1999;119:436–54. https://doi.org/10.1016/S0010-2180(99)00073-5.

Nomenclature

Symbols

E:	ATFM efficiency function
F:	ATFM dynamic thickening factor
F_{max}:	ATFM maximum thickening factor
N_{Thick}:	ATFM number of points within the thickened flame front
S_c:	Consumption speed [m/s]
L:	Integral turbulent length scale [m]
u:	Velocity [m/s]
Y:	Species mass fraction
Z:	Mixture fraction

Greek

α:	Solved strain rate [1/s]
b:	Temperature exponent
φ:	Generic quantity (species mass fraction of enthalpy)
μ:	Mean value
∇:	Gradient operator
σ:	Standard deviation
τ:	Time [ms]
Ω:	ATFM flame sensor
$\dot{\omega}$:	Chemical source term [kg/m^{3}s]

Subscripts

c:	Crossflow
j:	Jet
l:	Laminar
t:	Turbulent
sto:	Stochiometric

Acronyms:

AMR:	Automatic mesh refinement
ATFM:	Artificially thickened flame model
CFD:	Computational fluid dynamics
DLN:	Dry-Low NOx
DLR:	Deutsches Zentrum für Luft-und Raumfahrt
DNS:	Direct numerical simulation
FGM:	Flamelet generated manifold
FI:	Normalized flame index
FR:	Finite rate
FTT:	Flow through time
JFICF:	Jet flame in crossflow
JICF:	Jet in crossflow
GT:	Gas turbine
LES:	Large eddy simulation
LS:	Leeward side of the jet
PIV:	Particle Imagine Velocimeter
PLIF:	Planar Laser Induced Fluorescence
RANS:	Reynold-Averaged Navier Stokes
RMS:	Root mean square
SGS:	Subgrid scale
TI:	Takeno Index
WS:	Windward side of the jet